

1 August 8th, 2024,

2 Dear EarthArXiv Editors:

3 On behalf of myself and my co-authors, I submit our original research article “The Origin of Forearc
4 Depressions” for consideration for publication as a non-peer reviewed preprint in EarthArXiv. The
5 manuscript will be submitted to Terra Nova.

6 Please address all correspondence regarding this manuscript to me at chuqiaoh@sfu.ca.

7 Thank you for your consideration.

8 Sincerely,

9 Mr. Chuqiao Huang (chuqiaoh@sfu.ca)

10 Ph.D. Candidate, Simon Fraser University

11

12 Dr. Shahin E. Dashtgard (shahin_dashtgard@sfu.ca)

13 Professor, Simon Fraser University

14

15 Dr. H. Daniel Gibson (hdgibson@sfu.ca)

16 Professor, Simon Fraser University

17

18 Dr. Andrew J. Calvert (acalvert@sfu.ca)

19 Professor, Simon Fraser University

20

21 The origin of forearc depressions

22 **Chuqiao Huang¹, Shahin E. Dashtgard¹, H. Daniel Gibson¹, Andrew J. Calvert¹**

23 *¹Department of Earth Sciences, Simon Fraser University, 8888 University Dr., Burnaby, British*
24 *Columbia, Canada, V5A 1S6*

25 **Correspondence:** Chuqiao Huang (Chuqiaoh@sfu.ca)

26 **ABSTRACT**

27 Forearc depressions form over continental subduction zones with young, slowly subducting slabs and
28 thick trench fills. They are bound seaward by a coast range and landward by a volcanic arc such that
29 subsidence in forearc depressions occurs between orogens and in areas characterized by plate
30 convergence. We propose a model for forearc depression formation based on geophysical and seismic
31 data from four circum-Pacific subduction zones. Coast range crests coincide with >100 mGal gravity
32 anomalies, which are attributed to underplated material and indicate that underplating drives coast range
33 uplift. Coast range crests are situated near the down-dip termini of megathrust earthquake rupture zones,
34 showing that coast ranges overlie where subduction interface sliding behaviour transitions from frictional
35 to semi-frictional. This transition causes subduction interface shear stress to begin decreasing with depth
36 and triggers underplating as shear stress becomes insufficient to drag buoyant material deeper. Forearc
37 depressions are situated landward of inter-plate seismic phenomena, indicating they overlie the hydrated
38 forearc mantle. Forearc depressions form as counter-flexural basins over the hydrated forearc mantle; in
39 this position the upper plate crust is not supported by the flexurally rigid slab and can bend downwards.
40 Forearc depressions do not form over old slabs because old slabs do not exceed the temperature threshold
41 for semi-frictional sliding prior to intersecting the mantle wedge corner. Fast convergence rates and thin
42 trench fills promote subduction erosion along the subduction interface, thereby prohibiting the formation
43 of coast ranges, and by extension, forearc depressions.

44 INTRODUCTION

45 Forearc depressions (Fig. 1) are a type of forearc basin and form over continental subduction
46 zones with young (typically <30 Ma), slowly subducting (<65 mm yr⁻¹) slabs and thick trench sediment
47 fills (>2.5 km). Forearc depressions entirely overlie the upper plate and are bound seaward by a coast
48 range and landward by a volcanic arc. Modern examples include the Seto Inland Sea of the Nankai
49 subduction zone in Japan; the Kenai Lowlands–Cook Inlet–Shelikof Strait of the Alaskan subduction
50 zone in USA; the Salish–Puget–Willamette Lowland of the Cascadia subduction zone in Canada and
51 USA; and the Central Depression of the south-central Chilean subduction zone (Fig. 2).

52 Forearc depressions are narrow (typically 75 km trench-orthogonal width) with km-scale thick
53 basin fills and are sandwiched between areas of km-scale uplift. Their formation is challenging to explain
54 as proposed hypotheses must address how forearc depressions form between orogens and in regions
55 characterized by plate convergence. Recently, Menant et al. (2019, 2020) used computer modelling to
56 hypothesize that fluid escape from the subduction channel increases subduction interface shear stress,
57 which triggers underplating. Underplating drives coast range uplift, which then causes downwards
58 counter-flexure of the upper plate crust and forearc depression formation. Here, we revise the model of
59 Menant et al. (2019, 2020) using empirical data to show that changes in subduction interface rheology
60 decreases shear stress and triggers underplating, and that a young, slowly subducting slab and thick trench
61 cover are required for this process. We also show that forearc depressions are situated over the hydrated
62 forearc mantle and cannot form seaward of the mantle wedge corner. For clarity, we use ‘coast range’ to
63 refer to forearc highs that form through underplating and not through other mechanisms, such as over-
64 thrusting of the accretionary prism (e.g., the Sunda Subduction Zone; Mukti et al., 2021).

65 Subduction interface shear stress varies with depth and as a function of sliding behaviour. In warm
66 subduction zones, which includes those with young slabs, the subduction interface can be divided into

67 frictional, semi-frictional, and stable sliding domains (Fig. 1) and the locations of these domains can be
68 inferred by their differing seismic behaviours. Shear stress peaks and begins to decrease in the transition
69 between the frictional and semi-frictional domains (Gao and Wang, 2017).

70 In the frictional domain (Fig. 1), shear stress increases with depth (Gao and Wang, 2017) because
71 frictional strength increases with normal stress. The frictional domain defines the seismogenic zone
72 wherein megathrust earthquakes nucleate and propagate. The up-dip limit (seaward and shallower) of the
73 frictional domain depends on subduction interface temperature and mineralogy and can extend to the
74 seafloor (Roesner et al., 2020; Stanislawski et al., 2022). The down-dip limit (landward and deeper) of
75 the frictional domain corresponds to where the subduction interface exceeds 300–400 °C whereupon
76 quartz and feldspar begin to exhibit crystalline plasticity (Hyndman et al., 1997; Oleskevich et al., 1999).

77 In the semi-frictional domain (Fig. 1), shear stress decreases with depth (Gao and Wang, 2017)
78 because ductile strength decreases with temperature. Megathrust earthquakes cannot propagate into the
79 semi-frictional domain due to its rate-strengthening nature, and viscous processes cause slow-slip events
80 (Schwartz and Rokosky, 2007). Very young slabs (<20 Ma) additionally experience metamorphic
81 dehydration reactions at shallow depths (<50 km; Condit et al., 2020); this releases slab fluids that are
82 trapped beneath an impermeable subduction interface. Trapped fluids greatly lower shear stress (Gao and
83 Wang, 2017) and lowered shear stress generates episodic tremor and slip that clusters around the mantle
84 wedge corner (Shelly et al., 2006; Calvert et al., 2020).

85 In the stable-sliding domain (Fig. 1), shear stress is low and the subduction interface is aseismic.
86 The up-dip limit of the stable-sliding domain is where the slab contacts the hydrated forearc mantle and
87 free water is limited. Antigorite, the high pressure form of serpentinite (Schwartz et al., 2013), deforms
88 by viscous processes at inter-seismic strain rates (Tulley et al., 2022) and cannot accumulate the stress
89 required to initiate megathrust earthquakes.

90 Subduction interface shear stress is determined using the seismic behaviour of different sliding
91 domains, and hence, we examine geophysical and seismic data from subduction zones that host forearc
92 depressions. For each system, we compile data on topography and bathymetry, convergence rates, slab
93 ages, free-air gravitational anomalies, megathrust earthquake epicenter and rupture zones, tremor
94 epicenters, and top-of-slab depth (Supplementary Data File 1). We map and interpret these data to
95 establish how underplating, subduction interface shear stress distribution, and the location of the mantle
96 wedge corner drive coast range and forearc depression formation. We also show why young, slowly
97 subducting slabs and thick trench cover are required for coast range and forearc depression formation.

98 **CHARACTERIZATION OF FOREARC DEPRESSIONS**

99 In the Menant et al. (2019, 2020) model, underplating uplifts the overlying crust and generates a
100 coast range. Gravity anomalies increase towards the coast range crest to >100 mGal, and increasing
101 gravity anomalies are attributed to underplated material (Bassett and Watts, 2015) (Figs. 3A–D).
102 Specifically, underplating causes uncompensated crustal thickening, which increases free-air gravity
103 anomalies. Increasing gravity anomalies associated with coast ranges coincide with km-scale reflector
104 bands that are interpreted as underplated material (Calvert et al., 2006; Kimura et al., 2010; Scholl, 2021;
105 Delph et al., 2021).

106 Coast ranges also overlie where subduction interface shear stress begins to decrease with depth,
107 which is evident in the position of coast range topographic crests near the down-dip termini of megathrust
108 earthquake rupture zones (Figs. 3E–H). In warm subduction zones, megathrust earthquakes only
109 propagate in the frictional domain of the subduction interface (Fig. 1) and rupture zones terminate in the
110 transition between the frictional and semi-frictional domains. This transition is also where shear stress
111 changes from increasing with depth to decreasing with depth. There is no direct evidence from Cascadia
112 that shows the coast range overlying the down-dip termini of megathrust earthquake rupture zones

113 because the last megathrust earthquake occurred prior to modern record keeping (in 1700). However,
114 geodetically inferred interseismic locking models for Cascadia predict that subduction interface locking
115 (i.e., the predicted megathrust earthquake rupture zone) decreases to <10% beneath Cascadia's coast
116 range (Li et al., 2018; Lindsey et al., 2021), which is consistent with a transition from frictional to semi-
117 frictional sliding along the subduction interface.

118 The location of coast range topographic crests over where shear stress begins decreasing with
119 depth indicates that decreasing shear stress triggers the underplating necessary for coast range uplift.
120 Underplating occurs because shear stress becomes insufficient to drag buoyant material within the
121 subduction interface deeper.

122 All forearc depressions are situated landward of inter-plate seismic activity, showing they are
123 situated landward of the mantle wedge corner (Figs. 3E–H). In warm subduction zones, megathrust
124 earthquakes only propagate within the frictional sliding domain, which only exists where the slab is
125 beneath the upper plate crust and not the mantle (Fig. 1). As well, Nankai (Shelly et al., 2006) and
126 Cascadia (Calvert et al., 2020) experience episodic tremor and slip (Figs. 3E and G), and tremor
127 epicenters cluster around the mantle wedge corner (Fig. 1). The distribution of both megathrust
128 earthquake rupture zones and tremors seaward of forearc depressions show that all forearc depressions are
129 situated landward of the mantle wedge corner.

130 Underplating causes the overlying crust to flex upwards (Menant et al., 2020) and this upwards
131 flexure must be compensated by downwards flexure elsewhere. This cannot occur seaward of the mantle
132 wedge corner as the upper plate crust is supported through direct contact with the flexurally rigid slab.
133 Landward of the mantle wedge corner, the upper plate crust is no longer supported by physical contact
134 with the slab and so it can flex downwards to form the forearc depression.

135

136 The transition from frictional to semi-frictional sliding and the associated decrease in shear stress
137 that triggers underplating requires a young slab (<30 Ma; Fig. 2). Old slabs do not reach the temperature
138 threshold for transition between frictional and semi-frictional sliding prior to intersecting the mantle
139 wedge corner. As well, old slabs do not experience substantial metamorphic dehydration until they are
140 beneath the arc (Condit et al., 2020), which leads to a dry, antigorite-poor forearc mantle (Abers et al.,
141 2017; Wang et al., 2022). Consequently, old slabs are characterized by a single frictional domain wherein
142 shear stress increases with depth well into the forearc mantle. Old slabs also exhibit different seismic
143 behaviours: without a semi-frictional domain to resist the propagation of megathrust earthquakes
144 (Schwartz and Rokosky, 2007), rupture zones can extend into the hydrated forearc mantle (Brantut et al.,
145 2016). The exception to the relationship between slab age and subduction interface rheology described
146 above is Alaska, where the Pacific Plate is 35–50 Ma at the trench (Fig. 2B). The Pacific slab undergoes
147 flat subduction for 200–300 km over which it heats and exceeds 400 °C prior to intersecting the mantle
148 wedge corner (Qu et al., 2022).

149 A thick trench cover (>2.5 km) is required for coast range uplift through underplating because
150 trench sediments ultimately become the primary underplated material. For example, in the Central
151 American Subduction Zone, the subducting Cocos Plate is 0–25 Ma at the trench. The subduction zone
152 experiences SSEs and ETS (Baba et al., 2021), which shows the existence of a semi-frictional domain.
153 However, neither a coast range nor forearc depression are developed, and instead, a single, broad forearc
154 basin stretches from the shoreline to the trench. This is attributed to thin trench sediment cover (<0.5 km;
155 Clift and Vannucchi, 2004), which provides insufficient material to underplate and generate a coast range.
156 In contrast, subduction zones that host forearc depressions possess thick trench sediment covers (2.5–3.5
157 km; Clift and Vannucchi, 2004) which provide sufficient material for underplating.

158 Finally, a slow subduction rate ($<65 \text{ mm yr}^{-1}$; Fig. 2) is required for forearc depression formation.
159 At faster convergence rates, tectonic erosion dominates along the subduction interface (Clift and
160 Vannucchi, 2004) and underplating is suppressed; this inhibits the formation of a coast range.

161 **FORMATION OF FOREARC DEPRESSIONS**

162 Subduction zones with forearc depressions include an additional forearc basin over the
163 accretionary prism (Fig. 4). However, barring Nankai, for which subduction initiated recently (15 Ma;
164 Moreno et al., 2023), all subduction zones investigated here formerly comprised a single forearc basin
165 that stretched from the coastline to the trench. This is indicated by older strata within forearc depressions
166 that correlate to coeval strata over and/or seaward of the coast range (England and Bustin, 1998; Encinas
167 et al., 2012; LePain et al., 2014; Scanlon et al., 2021; Darin et al., 2022). For example, the Georgia Basin
168 is the northern-most forearc depression of Cascadia, and its basal succession is the Nanaimo Group, a >3
169 km thick succession of primarily Upper Cretaceous strata (England and Bustin, 1998; Girotto et al.,
170 2024). The Nanaimo Group is covered by >3 km of Cenozoic strata in the Georgia Basin; however,
171 Nanaimo Group strata, including trench orthogonal-oriented deep-marine turbidites, are exposed on
172 Vancouver Island, which is the associated coast range. This distribution of strata indicates that for much
173 of Nanaimo Group deposition, no trench-parallel topographic barrier existed, and sedimentation occurred
174 in a single, broad forearc basin. Based on this, we propose the following model for the formation of
175 forearc depressions (Fig. 4):

176 1) Prior to forearc depression formation, a single forearc basin stretches from the shoreline to the
177 trench and is dominated by deep-marine depositional systems and trench-orthogonal drainage
178 (e.g., south Cascadia in the Eocene; Santra et al., 2013). Coast range uplift is suppressed by
179 unsuitable subduction parameters such as an old slab, thin trench sediment cover, and/or high
180 convergence rate (Fig. 4A).

- 181 2) Increases in trench sedimentation, decreases in slab age, and/or decreases in convergence rate
182 initiate underplating. The accretionary prism grows, leading the frictional domain to shift seaward
183 as a thick blanket of sediment insulates the slab. Underplating focuses over the transition between
184 the frictional and semi-frictional domains, which uplifts the overlying crust to generate a coast
185 range. The coast range divides the overlying forearc basin in two (Fig. 4B).
- 186 3) Repeated underplating leads to further coast range uplift. Forearc strata overlying the coast range
187 are uplifted, eroded, and re-incorporated into the flanking forearc basins (e.g., south Cascadia in
188 the Oligocene; Darin et al., 2022). Flexural counter bending occurs over the hydrated forearc
189 mantle generating a forearc depression (Menant et al., 2020). Sedimentation in the forearc
190 depression is dominated by continental- and shallow-marine depositional systems and trench-
191 parallel drainage (Fig. 4C).

192 **ACKNOWLEDGEMENTS**

193 The authors thank the reviewers, ____, ____, and the editor ____, whose comments improved the
194 quality of this manuscript. The authors thank Kelin Wang of the Geological Society of Canada whose
195 ideas greatly improved this manuscript, and Evangeline Lapalme for her guidance with ArcGIS Pro. This
196 study was funded through a Natural Sciences and Engineering Research Council of Canada Discovery
197 Grant to Dr. Shahin Dashtgard (RGPIN-2019-04528).

198 **REFERENCES CITED**

- 199 Abers, G.A., van Keken, P.E., and Hacker, B.R., 2017, The cold and relatively dry nature of mantle
200 forearcs in subduction zones: *Nature Geoscience*, v. 10, p. 333–337, doi:10.1038/ngeo2922.
- 201 Baba, S., Obara, K., Takemura, S., Takeo, A., and Abers, G.A., 2021, Shallow Slow Earthquake Episodes
202 Near the Trench Axis off Costa Rica: *Journal of Geophysical Research: Solid Earth*, v. 126, p.
203 e2021JB021706, doi:10.1029/2021JB021706.

204 Bassett, D., and Watts, A.B., 2015, Gravity anomalies, crustal structure, and seismicity at subduction
205 zones: 2. Interrelationships between fore-arc structure and seismogenic behavior: CRUSTAL
206 STRUCTURE AND SEISMICITY: 2. FORE-ARC STRUCTURE: Geochemistry, Geophysics,
207 Geosystems, v. 16, p. 1541–1576, doi:10.1002/2014GC005685.

208 Brantut, N., Passelègue, F.X., Deldicque, D., Rouzaud, J.-N., and Schubnel, A., 2016, Dynamic
209 weakening and amorphization in serpentinite during laboratory earthquakes: *Geology*, v. 44, p.
210 607–610, doi:10.1130/G37932.1.

211 Calvert, A.J., Bostock, M.G., Savard, G., and Unsworth, M.J., 2020, Cascadia low frequency earthquakes
212 at the base of an overpressured subduction shear zone: *Nature Communications*, v. 11, p. 3874,
213 doi:10.1038/s41467-020-17609-3.

214 Calvert, A.J., Ramachandran, K., Kao, H., and Fisher, M.A., 2006, Local thickening of the Cascadia
215 forearc crust and the origin of seismic reflectors in the uppermost mantle: *Seismic Probing of*
216 *Continents and their Margins*, v. 420, p. 175–188, doi:10.1016/j.tecto.2006.01.021.

217 Clift, P., and Vannucchi, P., 2004, Controls on tectonic accretion versus erosion in subduction zones:
218 Implications for the origin and recycling of the continental crust: *Reviews of Geophysics*, v. 42,
219 doi:10.1029/2003RG000127.

220 Condit, C.B., Guevara, V.E., Delph, J.R., and French, M.E., 2020, Slab dehydration in warm subduction
221 zones at depths of episodic slip and tremor: *Earth and Planetary Science Letters*, v. 552, p.
222 116601, doi:10.1016/j.epsl.2020.116601.

223 Darin, M.H., Armentrout, J.M., and Dorsey, R.J., 2022, Oligocene onset of uplift and inversion of the
224 Cascadia forearc basin, southern Oregon Coast Range, USA: *Geology*, v. 50, p. 603–609,
225 doi:10.1130/G49925.1.

- 226 Delph, J.R., Thomas, A.M., and Levander, A., 2021, Subcretionary tectonics: Linking variability in the
227 expression of subduction along the Cascadia forearc: *Earth and Planetary Science Letters*, v. 556,
228 p. 116724, doi:10.1016/j.epsl.2020.116724.
- 229 Encinas, A., Finger, K.L., Buatois, L.A., and Peterson, D.E., 2012, Major forearc subsidence and deep-
230 marine Miocene sedimentation in the present Coastal Cordillera and Longitudinal Depression of
231 south-central Chile (38°30'S–41°45'S): *GSA Bulletin*, v. 124, p. 1262–1277,
232 doi:10.1130/B30567.1.
- 233 England, T.D.J., and Bustin, R.M., 1998, Architecture of the Georgia Basin southwestern British
234 Columbia: *Bulletin of Canadian Petroleum Geology*, v. 46, p. 288–320,
235 doi:10.35767/gscpgbull.46.2.288.
- 236 Gao, X., and Wang, K., 2017, Rheological separation of the megathrust seismogenic zone and episodic
237 tremor and slip: *Nature*, v. 543, p. 416–419, doi:10.1038/nature21389.
- 238 Giroto, K., Dashtgard, S.E., Huang, C., MacEachern, J.A., Gibson, H.D., and Cathyl-Huhn, G., 2024,
239 Stratigraphy, palaeogeography and evolution of the lower Nanaimo Group (Cretaceous), Georgia
240 Basin, Canada: *Basin Research*, v. 36, p. e12830, doi:10.1111/bre.12830.
- 241 Hyndman, R.D., Yamano, M., and Oleskevich, D.A., 1997, The seismogenic zone of subduction thrust
242 faults: *The Island Arc*, v. 6, p. 244–260, doi:10.1111/j.1440-1738.1997.tb00175.x.
- 243 Kimura, H., Takeda, T., Obara, K., and Kasahara, K., 2010, Seismic Evidence for Active Underplating
244 Below the Megathrust Earthquake Zone in Japan: *Science*, v. 329, p. 210–212,
245 doi:10.1126/science.1187115.
- 246 LePain, D.L., Stanley, R.G., Helmold, K.P., and Shellenbaum, D.P., 2014, Geologic Framework and
247 Petroleum Systems of Cook Inlet Basin, South-Central Alaska, *in* Stone, D.M. and Hite, D.M.

248 eds., Oil and Gas Fields of the Cook Inlet Basin, Alaska, American Association of Petroleum
249 Geologists, v. 104, p. 0, doi:10.1306/13491874M1043621.

250 Li, S., Wang, K., Wang, Y., Jiang, Y., and Dosso, S.E., 2018, Geodetically Inferred Locking State of the
251 Cascadia Megathrust Based on a Viscoelastic Earth Model: Journal of Geophysical Research:
252 Solid Earth, v. 123, p. 8056–8072, doi:10.1029/2018JB015620.

253 Lindsey, E.O., Mallick, R., Hubbard, J.A., Bradley, K.E., Almeida, R.V., Moore, J.D.P., Bürgmann, R.,
254 and Hill, E.M., 2021, Slip rate deficit and earthquake potential on shallow megathrusts: Nature
255 Geoscience, v. 14, p. 321–326, doi:10.1038/s41561-021-00736-x.

256 Menant, A., Angiboust, S., and Gerya, T., 2019, Stress-driven fluid flow controls long-term megathrust
257 strength and deep accretionary dynamics: Scientific Reports, v. 9, p. 9714, doi:10.1038/s41598-
258 019-46191-y.

259 Menant, A., Angiboust, S., Gerya, T., Lacassin, R., Simoes, M., and Grandin, R., 2020, Transient
260 stripping of subducting slabs controls periodic forearc uplift: Nature Communications, v. 11, p.
261 1823, doi:10.1038/s41467-020-15580-7.

262 Moreno, E.J., Manea, V.C., Manea, M., Yoshioka, S., Suenaga, N., and Bayona, A., 2023, Numerical
263 modeling of subduction and evaluation of Philippine Sea Plate tectonic history along the Nankai
264 Trough: Scientific Reports, v. 13, p. 18313, doi:10.1038/s41598-023-45370-2.

265 Mukti, M.M., Maulin, H.B., and Permana, H., 2021, Growth of forearc highs and basins in the oblique
266 Sumatra subduction system: Petroleum Exploration and Development, v. 48, p. 683–692,
267 doi:10.1016/S1876-3804(21)60054-X.

268 Oleskevich, D.A., Hyndman, R.D., and Wang, K., 1999, The updip and downdip limits to great
269 subduction earthquakes: Thermal and structural models of Cascadia, south Alaska, SW Japan, and

270 Chile: *Journal of Geophysical Research: Solid Earth*, v. 104, p. 14965–14991,
271 doi:10.1029/1999JB900060.

272 Qu, R., Ji, Y., Zhu, W., Zhao, Y., and Zhu, Y., 2022, Fast and Slow Earthquakes in Alaska: Implications
273 from a Three-Dimensional Thermal Regime and Slab Metamorphism: *Applied Sciences*, v. 12, p.
274 11139, doi:10.3390/app122111139.

275 Roesner, A., Ikari, M.J., Saffer, D.M., Stanislawski, K., Eijsink, A.M., and Kopf, A.J., 2020, Friction
276 experiments under in-situ stress reveal unexpected velocity-weakening in Nankai accretionary
277 prism samples: *Earth and Planetary Science Letters*, v. 538, p. 116180,
278 doi:10.1016/j.epsl.2020.116180.

279 Santra, M., Steel, R.J., Olariu, C., and Sweet, M.L., 2013, Stages of sedimentary prism development on a
280 convergent margin — Eocene Tyee Forearc Basin, Coast Range, Oregon, USA: From Source to
281 Sink - Quantifying the mass transfer from mountain ranges to sedimentary basins, v. 103, p. 207–
282 231, doi:10.1016/j.gloplacha.2012.11.006.

283 Scanlon, D.P., Bershaw, J., Wells, R.E., and Streig, A.R., 2021, The spatial and temporal evolution of the
284 Portland and Tualatin forearc basins, Oregon, USA: *Geosphere*, v. 17, p. 804–823,
285 doi:10.1130/GES02298.1.

286 Scholl, D.W., 2021, Seismic imaging evidence that forearc underplating built the accretionary rock record
287 of coastal North and South America: *Geological Magazine*, v. 158, p. 104–117,
288 doi:10.1017/S0016756819000955.

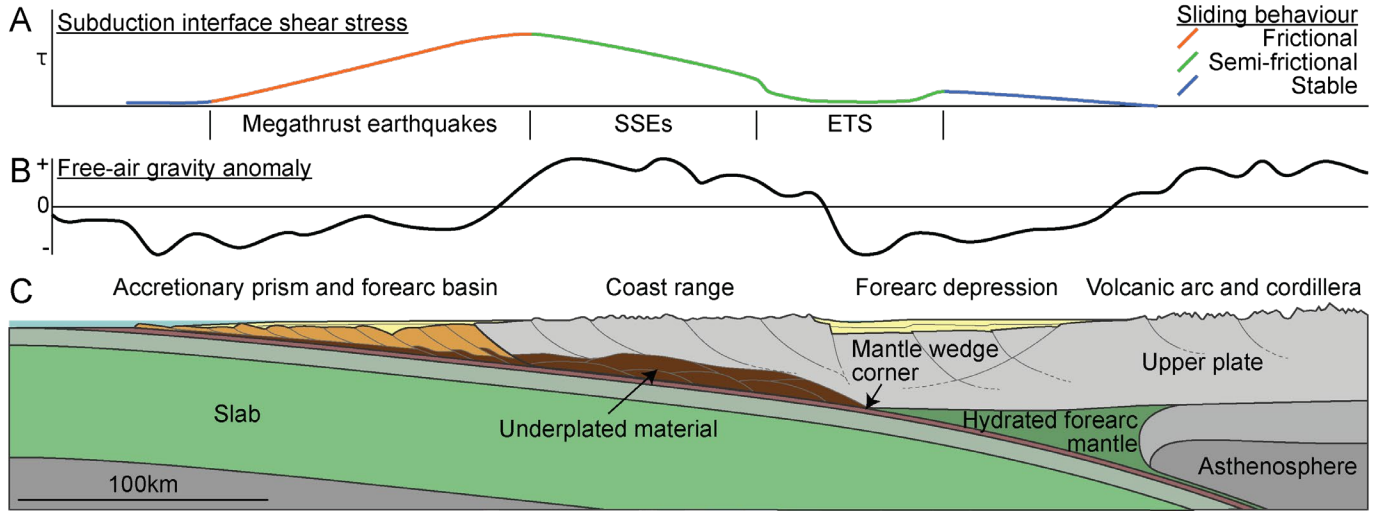
289 Schwartz, S., Guillot, S., Reynard, B., Lafay, R., Debret, B., Nicollet, C., Lanari, P., and Auzende, A.L.,
290 2013, Pressure–temperature estimates of the lizardite/antigorite transition in high pressure
291 serpentinites: *Lithos*, v. 178, p. 197–210, doi:10.1016/j.lithos.2012.11.023.

- 292 Schwartz, S.Y., and Rokosky, J.M., 2007, Slow slip events and seismic tremor at circum-Pacific
293 subduction zones: SLOW SLIP AND SEISMIC TREMOR: Reviews of Geophysics, v. 45, p. n/a-
294 n/a, doi:10.1029/2006RG000208.
- 295 Shelly, D.R., Beroza, G.C., Ide, S., and Nakamura, S., 2006, Low-frequency earthquakes in Shikoku,
296 Japan, and their relationship to episodic tremor and slip: Nature, v. 442, p. 188–191,
297 doi:10.1038/nature04931.
- 298 Stanislawski, K., Roesner, A., and Ikari, M.J., 2022, Implications for megathrust slip behavior and pore
299 pressure at the shallow northern Cascadia subduction zone from laboratory friction experiments:
300 Earth and Planetary Science Letters, v. 578, p. 117297, doi:10.1016/j.epsl.2021.117297.
- 301 Tulley, C.J., Fagereng, Å., Ujiie, K., Piazzolo, S., Tarling, M.S., and Mori, Y., 2022, Rheology of
302 Naturally Deformed Antigorite Serpentinite: Strain and Strain-Rate Dependence at Mantle-Wedge
303 Conditions: Geophysical Research Letters, v. 49, p. e2022GL098945,
304 doi:10.1029/2022GL098945.
- 305 Wang, D., Wang, L., Zhang, R., Cai, N., Zhang, J., Chen, P., and Cao, Y., 2022, Mantle Wedge Water
306 Contents Estimated From Ultrasonic Laboratory Measurements of Olivine-Antigorite Aggregates:
307 Geophysical Research Letters, v. 49, p. e2022GL098226, doi:10.1029/2022GL098226.

308

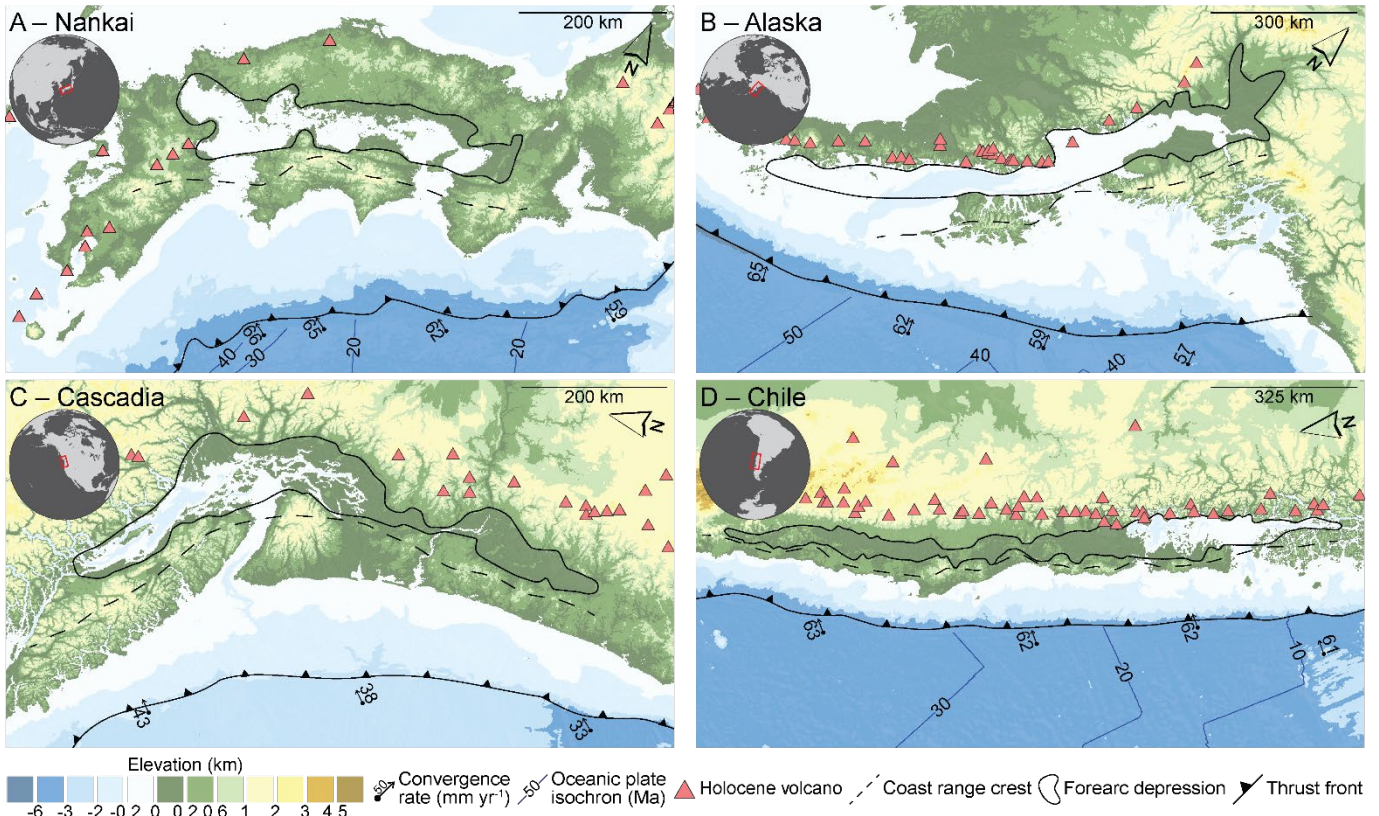
309

310 **FIGURES AND CAPTIONS**



311

312 **Figure 1.** Schematic cross-section of a warm subduction zone hosting a forearc depression. **A)** Shear
313 stress (τ) distribution along the subduction interface and predicted inter-plate sliding behaviour. Expected
314 locations of inter-plate seismic events are labelled on the x-axis. Abbreviations: SSEs – slow slip events;
315 ETS – episodic tremor and slip. **B)** Predicted free-air gravity anomaly field of the subduction zone. **C)**
316 Major tectonic elements of the subduction zone. No vertical exaggeration.



317

318

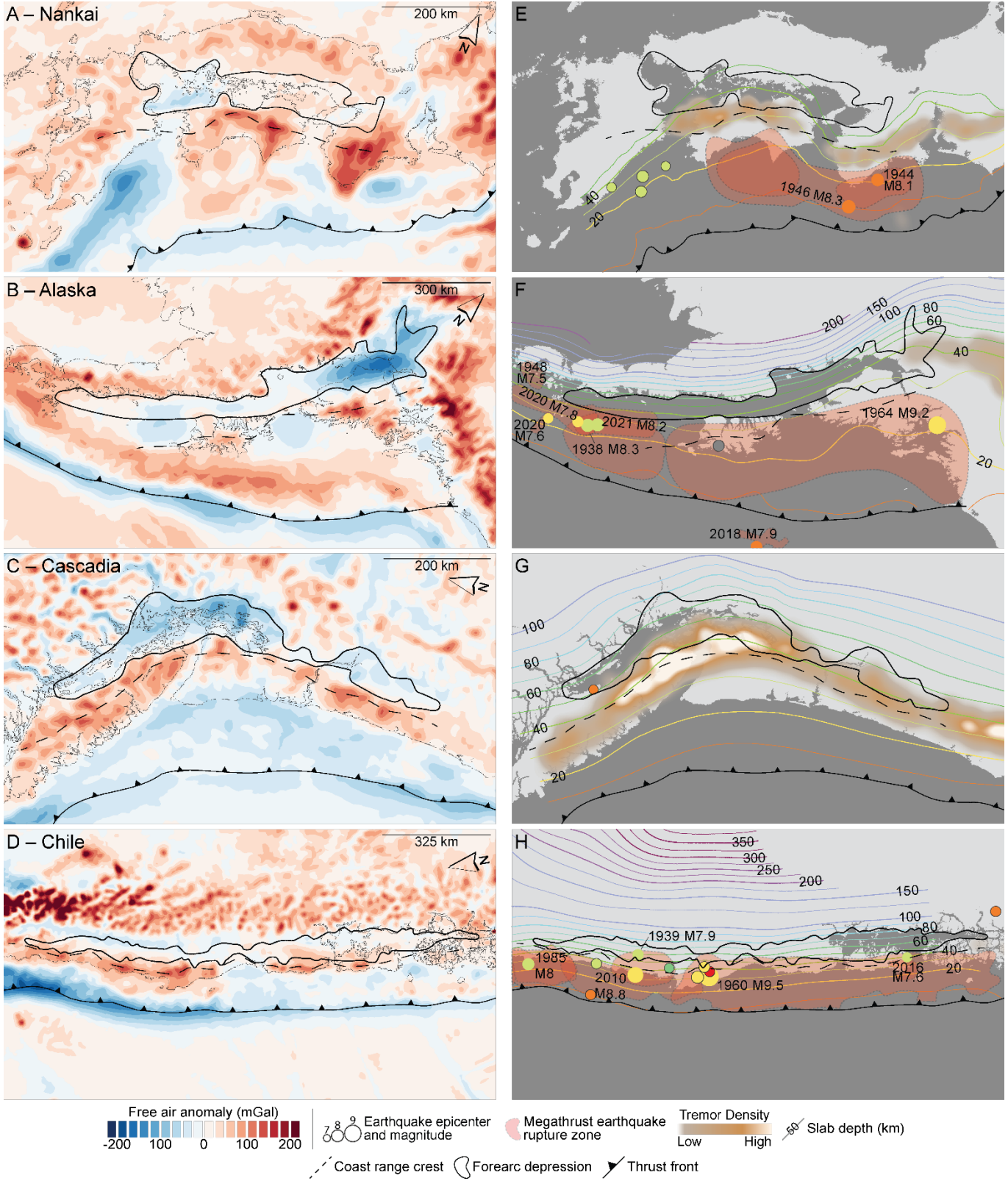
319

320

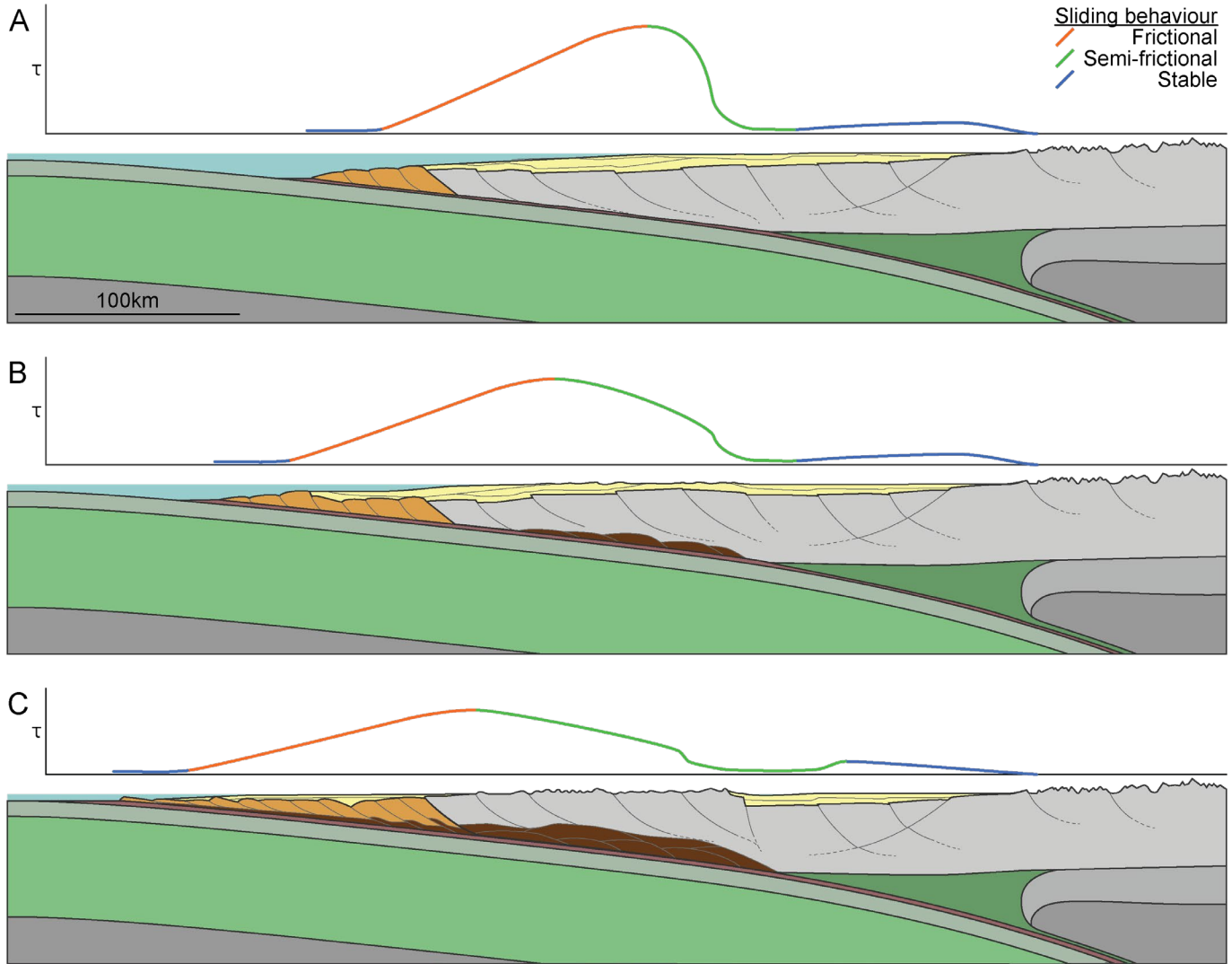
321

322

Figure 2. General subduction parameters of subduction zones with forearc depressions. Data shown include topography/bathymetry, convergence rate with respect to a stable upper plate, oceanic plate isochrons, Holocene volcanoes, coast range topographic crest, forearc depression boundary, and subduction thrust front. No oceanic plate isochrons are present for Cascadia because the Juan de Fuca oceanic plate is younger than 10 Ma everywhere.



324 **Figure 3.** Geophysical and seismic data from subduction zones with forearc depressions. All maps
325 include coast range topographic crest, forearc depression boundary, and subduction thrust front. **A–D)**
326 Free-air gravity anomalies, scaled to ± 200 mGal. **E – H)** Seismic activity. Data show include megathrust
327 earthquake magnitudes, epicenters, and rupture zones, tremor densities, and top-of-slab depth. Megathrust
328 earthquake epicenters and top-of-slab depth share the same colour scheme, which indicates depth. For
329 megathrust earthquake epicenters, no circle outline means its rupture zone is depicted and an outline
330 means it is not.
331



334 **Figure 4.** Schematic for the formation of a forearc depression. Time steps A–C are described in the text.
 335 Each schematic depicts the shear stress (τ) distribution along the subduction interface and predicted inter-
 336 plate sliding behaviour, and tectonic elements of the subduction zone. Legend and scale are same as
 337 figure 1. No vertical exaggeration.

338 **SUPPLEMENTARY FILE 1: DATA SOURCES**

339 Our study compiles and interprets publicly available data. We focus on four subduction zones
340 globally that host forearc depressions: Nankai, Alaska, Cascadia, and Chile. For each subduction zone,
341 we assemble and interpret three datasets: 1) general subduction parameters, 2) gravity, and 3) seismic.

342 **GENERAL SUBDUCTION PARAMETERS**

343 The general subduction parameters dataset comprises topographic and bathymetric data, forearc
344 depression boundaries, Holocene volcanic centers, oceanic plate isochrons, and plate convergence rates.
345 Topographic and bathymetric data are derived from the General Bathymetric Chart of the Oceans project
346 (Mayer et al., 2018). Coast ranges are defined by tracing a line through the topographic crest of each
347 coast range, and forearc depression boundaries are defined by tracing the 200m topographic contour.
348 Holocene volcanic data is derived from the Volcanoes of the World Database (Venzke, 2023), and
349 oceanic plate isochrons are derived from Seton et al., 2020. Plate convergence vectors are based on plate
350 motions calculated by the Global Strain Rate Model v2.1 (Kreemer et al., 2014) and are defined with
351 respect to a stable upper plate: for Nankai, the Philippine Sea Plate subducts beneath the stable Amur
352 Plate; for Alaska, the Pacific Plate subducts beneath the stable North American Plate; for Cascadia, the
353 Juan de Fuca Plate subducts beneath the stable North American Plate; and for Chile, the Nazca Plate
354 subducts beneath the stable South American Plate.

355 **GRAVITY DATA**

356 Gravity data is derived from the satellite free-air gravity model of Sandwell et al. (2014).
357 Sandwell et al. (2014) provide data in a 1 arc-minute by 1 arc-minute grid. We use kriging to generate our
358 free-air gravity anomaly map. We normalize all gravity data to ± 200 mGal because these values cover the
359 full range of gravity anomalies from the trench to the volcanic arcs of the subduction zones investigated

360 herein. While some areas, such as the Bonin trench and volcanic arc (Fig. 3A), have anomalies more than
361 ± 300 mGal, these higher values are not portrayed because they are not relevant to this study.

362 **SEISMIC DATA**

363 Seismic data includes megathrust earthquake epicenters and rupture zones, tremor epicenters, and
364 top-of-slab depth data. Megathrust earthquake epicenters are derived from the USGS earthquake catalog
365 for all earthquakes that: 1) occurred between 1900 and 2023, 2) exceeded 7.5 magnitude; and, 3) were
366 shallower than 70 km. These search parameters filter out most other earthquake types that occur near
367 subduction zones, such as intra-slab and intra-crust earthquakes. Megathrust rupture zone data are
368 compiled from a variety of sources. For Nankai, rupture zones are calculated by Ando (1975). For Alaska,
369 rupture zones are derived from the Alaska Earthquake Center. For Chile, rupture zones are compiled from
370 Kelleher (1972), Sparkes et al. (2010), and Hicks et al. (2014).

371 Tremor data is compiled from multiple sources. For Nankai, tremor data is from the World
372 Tremor Database generated by Idehara et al. (2014). For Alaska, tremors are from Wech (2016). For
373 Cascadia, tremors are derived from the Pacific Northwest Seismic Network's tremor catalog (Wech,
374 2021) for all events occurring between August 6, 2009 and September 4, 2023. For Chile, tremor data are
375 derived from the World Tremor Database, which combines data from Idehara et al. (2014), Yabe and Ide
376 (2014), and Pastén-Araya et al. (2022) . Slab depth data are from Nakanishi et al. (2018) for Nankai,
377 McCrory et al. (2012) for Cascadia, and the Slab 2.0 model of Hayes et al. (2018) for Alaska and Chile.

378

379 **BIBLIOGRAPHY**

- 380 Alaska Earthquake Center, 2023, Earthquake Map:, <https://earthquake.alaska.edu/earthquakes>.
- 381 Ando, M., 1975, Source mechanisms and tectonic significance of historical earthquakes along the nankai
382 trough, Japan: *Tectonophysics*, v. 27, p. 119–140, doi:10.1016/0040-1951(75)90102-X.
- 383 Hayes, G.P., Moore, G.L., Portner, D.E., Hearne, M., Flamme, H., Furtney, M., and Smoczyk, G.M.,
384 2018, Slab2, a comprehensive subduction zone geometry model: *Science*, v. 362, p. 58–61,
385 doi:10.1126/science.aat4723.
- 386 Hicks, S.P., Rietbrock, A., Ryder, I.M.A., Lee, C.-S., and Miller, M., 2014, Anatomy of a megathrust:
387 The 2010 M8.8 Maule, Chile earthquake rupture zone imaged using seismic tomography: *Earth
388 and Planetary Science Letters*, v. 405, p. 142–155, doi:10.1016/j.epsl.2014.08.028.
- 389 Idehara, K., Yabe, S., and Ide, S., 2014, Regional and global variations in the temporal clustering of
390 tectonic tremor activity: *Earth, Planets and Space*, v. 66, p. 66, doi:10.1186/1880-5981-66-66.
- 391 Kelleher, J.A., 1972, Rupture zones of large South American earthquakes and some predictions: *Journal
392 of Geophysical Research (1896-1977)*, v. 77, p. 2087–2103, doi:10.1029/JB077i011p02087.
- 393 Kreemer, C., Blewitt, G., and Klein, E.C., 2014, A geodetic plate motion and Global Strain Rate Model:
394 *Geochemistry, Geophysics, Geosystems*, v. 15, p. 3849–3889, doi:10.1002/2014GC005407.
- 395 Mayer, L., Jakobsson, M., Allen, G., Dorschel, B., Falconer, R., Ferrini, V., Lamarche, G., Snaith, H.,
396 and Weatherall, P., 2018, The Nippon Foundation—GEBCO Seabed 2030 Project: The Quest to
397 See the World’s Oceans Completely Mapped by 2030: *Geosciences*, v. 8,
398 doi:10.3390/geosciences8020063.
- 399 McCrory, P.A., Blair, J.L., Waldhauser, F., and Oppenheimer, D.H., 2012, Juan de Fuca slab geometry
400 and its relation to Wadati-Benioff zone seismicity: *Journal of Geophysical Research: Solid Earth*,
401 v. 117, doi:10.1029/2012JB009407.

402 Nakanishi, A., Takahashi, N., Yamamoto, Y., Takahashi, T., Ozgur Citak, S., Nakamura, T., Obana, K.,
403 Kodaira, S., and Kaneda, Y., 2018, Three-dimensional plate geometry and P-wave velocity
404 models of the subduction zone in SW Japan: Implications for seismogenesis, *in* Byrne, T.,
405 Underwood, M.B., III, Fisher, D., McNeill, L., Saffer, D., Ujiie, K., and Yamaguchi, A. eds.,
406 Geology and Tectonics of Subduction Zones: A Tribute to Gaku Kimura, Geological Society of
407 America, v. 534, p. 0, doi:10.1130/2018.2534(04).

408 Pastén-Araya, F. et al., 2022, Along-Dip Segmentation of the Slip Behavior and Rheology of the Copiapó
409 Ridge Subducted in North-Central Chile: Geophysical Research Letters, v. 49, p.
410 e2021GL095471, doi:10.1029/2021GL095471.

411 Sandwell, D.T., Müller, R.D., Smith, W.H.F., Garcia, E., and Francis, R., 2014, New global marine
412 gravity model from CryoSat-2 and Jason-1 reveals buried tectonic structure: Science, v. 346, p.
413 65–67, doi:10.1126/science.1258213.

414 Seton, M., Müller, R.D., Zahirovic, S., Williams, S., Wright, N.M., Cannon, J., Whittaker, J.M.,
415 Matthews, K.J., and McGirr, R., 2020, A Global Data Set of Present-Day Oceanic Crustal Age
416 and Seafloor Spreading Parameters: Geochemistry, Geophysics, Geosystems, v. 21, p.
417 e2020GC009214, doi:10.1029/2020GC009214.

418 Sparkes, R., Tilmann, F., Hovius, N., and Hillier, J., 2010, Subducted seafloor relief stops rupture in
419 South American great earthquakes: Implications for rupture behaviour in the 2010 Maule, Chile
420 earthquake: Earth and Planetary Science Letters, v. 298, p. 89–94, doi:10.1016/j.epsl.2010.07.029.

421 United States Geological Survey USGS Earthquake Catalog:,
422 <https://earthquake.usgs.gov/earthquakes/search/>.

423 Venzke, E., 2023, Volcanoes of the World:, doi:<https://doi.org/10.5479/si.GVP.VOTW5-2023.5.1>.

424 Wech, A.G., 2021, Cataloging Tectonic Tremor Energy Radiation in the Cascadia Subduction Zone:
425 Journal of Geophysical Research: Solid Earth, v. 126, p. e2021JB022523,
426 doi:10.1029/2021JB022523.

427 Wech, A.G., 2016, Extending Alaska's plate boundary: Tectonic tremor generated by Yakutat
428 subduction: Geology, v. 44, p. 587–590, doi:10.1130/G37817.1.

429 Yabe, S., and Ide, S., 2014, Spatial distribution of seismic energy rate of tectonic tremors in subduction
430 zones: Journal of Geophysical Research: Solid Earth, v. 119, p. 8171–8185,
431 doi:10.1002/2014JB011383.

432